A Bivalent Dissectional Analysis of the High-Affinity Interactions between Cdc42 and the Cdc42/Rac Interactive Binding Domains of Signaling Kinases in *Candida albicans*†

Zhengding Su,‡ Michael J. Osborne,‡ Ping Xu, Xiaolong Xu, Yang Li, and Feng Ni*

Biomolecular NMR and Protein Research Group, Biotechnology Research Institute, National Research Council of Canada, 6100 Royalmount Avenue, Montreal, Quebec, Canada H4P 2R2

Received May 6, 2005; Revised Manuscript Received September 14, 2005

ABSTRACT: The small GTPase Cdc42, a member of the highly conserved Rho family of intracellular GTPases, communicates with downstream signaling proteins via high-affinity interactions with the consensus Cdc42/Rac interactive binding (CRIB) polypeptide sequence. Previous biochemical and structural studies show that the CRIB motif itself is insufficient for high-affinity binding to Cdc42 but requires the sequence segment C-terminal to the CRIB motif for enhanced affinity. In this study, we have investigated the high-affinity (K_d in units of nanomolar) associations of two highly homologous extended CRIB domains (eCRIBs) from the PAK kinases, Cla4 and Cst20, with Cdc42 from *Candida albicans*. $^{1}H-^{15}N$ NMR heteronuclear NOE data of the eCRIB polypeptides in complex with *Candida* Cdc42 (CaCdc42) indicate that both eCRIB peptides have approximately two binding loci for CaCdc42. When each of the two eCRIB peptides is dissected into two fragments, the N-terminal fragments containing the minimal CRIB motif (mCRIB), mCla4 and mCst20, have relatively high binding affinities with dissociation constants (K_d) of 4.2 and 0.43 μM, respectively. On the other hand, the C-terminal fragments (cCRIB), cCla4 and cCst20, exhibit significantly lower affinities for their binding to CaCdc42. The cCla4 peptide binds to CaCdc42 with a sub-millimolar K_d of 275 μM, and the cCst20 peptide shows an even lower binding affinity (K_d = 1160 μM). Cross-titration experiments with the cognate fragments show that the binding affinity of cCst20 is enhanced ~5.5-fold (K_d = 207 μM) in the presence of saturating amounts of mCst20, and vice versa. No such effect is observed for the binding of cCla4 and mCla4. These results suggest that the Cdc42−CRIB system can be represented by a "dual recognition" model for protein−protein interactions [Kleanthous, C., et al. (1998) *Mol. Microbiol. 28*, 227−233], following much the same mechanisms of multivalent molecular interactions [Song, J., and Ni, F. (1998) *Biochem. Cell Biol. 76*, 177−188; Mammen, M., et al. (1998) *Angew Chem., Int. Ed. 37*, 2754−2794]. The bivalent modeling of linked peptide fragments shows that the binding of eCla4 follows a simple additivity/avidity model, while binding of eCst20 appears to have a more complex mechanism involving cooperative effects. The differential binding mechanisms between closely related eCRIB polypeptides and CaCdc42 provide a new molecular basis for understanding kinase activation and for the design of antifungal agents targeting the large protein interaction interfaces engaged by the fungal GTPase.

Cdc42 is an ancient, highly conserved, Rho-type small GTPase of the Ras superfamily of GDP/GTP-binding proteins. It plays an essential role in mediating intracellular signaling, triggering changes in transcription and in the actin cytoskeleton (*1*, *2*). In particular, the signaling pathway involving Cdc42 controls eukaryotic cell polarity by affecting the polymerization and distribution of actin in the cell cortex (*3*, *4*). Upon activation, Cdc42 interacts with a myriad of downstream effectors to regulate a diverse set of cellular functions. In mammalian cells, as many as 20 types of effectors have been identified to bind to Cdc42 and transduce the Cdc42-dependent signals downstream to ultimate destinations (*5*). Among this large group of effectors are protein kinases, lipid kinases, hydrolases and phosphatases, actin-bundling proteins, coatomers (vesicle coat proteins), adaptor proteins, and proteins that interact with members of the Arp2/3 complex and hence the actin cytoskeleton. Many of these effectors contain a conserved 18-amino acid sequence motif that has been named CRIB[1] (Cdc42/Rac interactive binding) domain, PBD (p21-binding domain), or GBD

† This work was supported by the Genomics and Health Initiative (GHI) of the National Research Council of Canada (NRCC Publication 47484), sponsored by the Government of Canada.

* To whom correspondence should be addressed. Telephone: (514) 496-6729. Fax: (514) 496-5143. E-mail: fengni@bri.nrc.ca.

‡ These authors contributed equally to this work.

[1] Abbreviations: CRIB, Cdc42/Rac interactive binding; eCRIB, extended CRIB domain; mCRIB, minimal CRIB; cCRIB, C-terminal region of eCRIB; AID, autoinhibitory domain; PDB, p21-binding domain; GDB, GTPase-binding domain; PAK, p21-activated kinase; ACK, Cdc42-associated protein kinase; WASP, Wiscott−Adrich syndrome protein; sNBD, succidinimidyl 6-[(7-nitrobenz-2-oxa-1,3-diazol-4-yl)amino]hexanoate; IPTG, isopropyl 1-thio-β-D-galactopyranoside; NMR, nuclear magnetic resonance; HSQC, heteronuclear single-quantum coherence; NOE, nuclear Overhauser effect.

10.1021/bi050846l CCC: $30.25 Published 2005 by the American Chemical Society
Published on Web 11/23/2005

(GTPase-binding domain) (*6*). For example, the CRIB motif exists in protein kinases PAK, MRCK, and ACK, adaptor proteins SPEC and WASP, and kinases MLK and MEKK4, adaptor Par6, scaffold protein IRSp53, and the Borg proteins (*1*).

PAK, ACK, and WASP are the most extensively studied CRIB motif-containing proteins that have provided the structural basis for our understanding of the interactions of the CRIB domains with Cdc42. Previous studies have shown that the consensus CRIB motif itself in PAK or WASP is insufficient for tight binding to Cdc42 and requires residues C-terminal to the CRIB motif for high-affinity interactions (*7*, *8*). This extended CRIB (eCRIB) fragment exhibits similar high affinities for Cdc42 compared to the full-length kinases (*9*), providing an excellent model for exploring the mechanism of binding of Cdc42 to downstream effector proteins. The eCRIB sequence in these proteins also contains part of a conserved autoinhibitory domain (AID) that together with the CRIB motif maintains the entire protein in inactive conformations (*9*−*11*). Upon binding to Cdc42, the eCRIB sequence appears to undergo a conformational change, triggering the activation of the autoinhibited proteins (*12*, *13*). A number of eCRIB polypeptides have been shown to form a complex with Cdc42 via a large and shallow interaction surface (*14*−*18*). Detailed binding mechanisms of the eCRIB polypeptides for Cdc42 have remained elusive even though sequence and amino acid determinants have been identified for conferring high-affinity protein−protein interactions (*7*, *8*, *19*). Such extensive interactions at protein−protein interfaces also appear to be a widespread structural feature in many protein complexes (*20*, *21*). The generally large molecular interfaces in these high-affinity protein complexes appear to have made it difficult to design small molecule inhibitors of many signaling protein−protein interactions (*22*, *23*).

In the pathogenic yeast *Candida albicans*, the PAK kinases, CaCla4 and Cst20, have been shown to be essential for virulence and morphological switching of the yeast to hyphal transition (*24*, *25*). Both kinases are structurally and functionally homologous to the Ste20 protein of *Saccharomyces cerevisiae*, which is a founding member of the p21-activated kinase (PAK) family (*26*, *27*). Like that of PAKs, the kinase activity of Ste20 is activated by its binding to Cdc42 (*9*, *28*). On the other hand, *Candida* Cdc42 (CaCdc42) is required for polarized growth of the pathogenic yeast through its interaction with both CaCla4 and Cst20. The activity of the small GTPase CaCdc42, rather than its expression, is the primary means through which CaCdc42 influences cellular morphogenesis (*29*, *30*).

Previously, we have investigated the specific, though weaker, binding of the consensus CRIB motif from human PAK1 to human Cdc42 (*31*). More recent studies revealed that even a high-affinity Cdc42−CRIB complex can exhibit very different mobilities between the consensus CRIB region and the affinity-enhancing sequence segment C-terminal to the CRIB motif (*32*). High structure order of the consensus CRIB region in complex with Cdc42 (*32*) is strongly correlated with the specific binding of peptide fragments containing the minimal CRIB sequence (*31*). The generally reduced structure order, or increased mobility, for the affinity-enhancing sequence segment appears to be accompanied by elevated mobilities of the surface areas of Cdc42 in close contact with the binding peptide (*32*). Such "concerted" and localized motions within the high-affinity Cdc42−CRIB complex point to conformational restriction as a potential way of reducing the binding affinities of Cdc42 with effector proteins (*32*). Given the large contact areas between Cdc42 and the extended CRIB peptides (*14*−*18*), segmental mobilities within the Cdc42−CRIB complex may also represent a mechanism for limiting the binding affinities of the Cdc42−CRIB complex to the observed nanomolar (nM) levels. In general, it remains unclear how and in what way affinity enhancement can be conferred by sequence extensions beyond the consensus CRIB sequence. Starting from ^{15}N NMR relaxation data, we therefore dissected the extended CRIB domains of the two *Candida* kinases, CaCla4 and Cst20, into two binding fragments as a way of analyzing systematically the mechanism of high-affinity interactions engaged by the CRIB polypeptides. Fluorescence and ^{15}N HSQC NMR titrations were used to determine the binding affinities of each constituent peptide. The results presented here indicate that peptide extensions C-terminal to the CRIB consensus sequence all have very weak intrinsic binding affinities for *Candida* Cdc42. In addition, these peptide sequences were found to enhance the binding affinities of extended CRIB domains to *Candida* Cdc42 through distinct and different binding mechanisms even for two closely related CRIB polypeptides, thus providing new insights into the signal transduction mechanisms of the Cdc42 protein.

EXPERIMENTAL PROCEDURES

Protein Expression. DNA fragments encoding the Cdc42 protein (residues 1−178) of *C. albicans* SC5314 were amplified from the genomic DNA by a standard PCR using the *pfu* polymerase. Through PCRs, two restriction sites, *Nde*I and *Bam*HI, were generated at the 5′-end and 3′-end, respectively. A stop codon, TAG, was placed immediately after the codon for residue 178. The PCR fragment was subcloned into pET-15b (Novagen, Madison, WI), and the resulting construct was defined as pCaCdc42Δ13 (W. Stevens and F. Ni, unpublished data). A CaCdc42 expression vector encoding the R150K mutation was constructed by use of the QuickChange site-directed mutagenesis kit (Stratagene, La Jolla, CA). The sequences of the wild-type and R150K mutant CaCdc42 vectors were verified by DNA sequencing.

Wild-type and mutant CaCdc42 proteins were expressed in the *Escherichia coli* BL21 strain as hexahistidine fusion proteins. For heteronuclear NMR experiments, CaCdc42 was uniformly labeled with ^{15}N, ^{15}N and ^{13}C, or ^{15}N, ^{13}C, and ^{2}H in M9 (in 99.9% D_2O for perdeuteration) minimal medium with BME vitamins (Sigma, St. Louis, MO) containing 2 g/L $(^{15}NH_4)_2SO_4$ and 2 g/L [$^{13}C_6$]glucose as the sole sources of nitrogen and carbon, respectively. Unlabeled CaCdc42 was grown in Luria broth. Cells were harvested from a 1 L culture by centrifugation at 8000*g* for 30 min and resuspended in 50 mL of lysis buffer [20 mM Tris-HCl (pH 8.0), 500 mM NaCl, 10 mM imidazole, 5 mM $MgCl_2$, 100 μM GDP, 2 μg/mL aprotinin, leupeptin, and pepstatin, and 10 μg/mL benzamidine and PMSF]. The collected cells were treated with lysozyme (1 mg/mL) for 30 min on ice, followed by sonication for 4 min and subsequent addition of DNase at 2 μg/mL. The insoluble fraction was removed by centrifugation at 10000*g* for 30 min. The supernatant was mixed with Ni−NTA agarose beads (Qiagen, Mississauga, ON) by rocking

for 1 h and then washed extensively in a column with a washing buffer [20 mM Tris-HCl (pH 8.0), 500 mM NaCl, 15 mM imidazole, and 5 mM $MgCl_2$]. The fusion protein was eluted with the wash buffer (50 mL) except that the concentration of imidazole was 200 mM. The protein sample was buffer-exchanged extensively using a CentriPrep YM10 apparatus to remove imidazole.

Nucleotide Exchange. The nonhydrolyzable GTP analogues GMPPNP and GMPPCP (Sigma) were used to produce the activated but stable nucleotide-loaded form of CaCdc42. In our work, no differences were observed for the two GTP analogue-loaded forms of Cdc42 in NMR titration and fluorescence experiments except that the lifetime of the complex with GMPPCP is longer than that with GMPPNP. Therefore, we switched to the use of GMPPCP instead of GMPPNP in later phases of the work, though the CaCdc42−GMPPNP complex was stable enough for NMR spectral assignments.

Nucleotide exchange was facilitated by incubating CaCdc42 with a 5−10-fold molar excess of the nonhydrolyzable GTP analogue in the presence of 10 mM EDTA. To this mixture was added 100 units of alkaline phosphatase beads, and the mixture was gently shaken on ice for 3 h. The alkaline phosphatase beads were removed by filtration, followed by the addition of $MgCl_2$ to a final concentration of 15 mM. The excess unbound nucleotides were removed using a PD-10 gel filtration column (Amersham Bioscience, Piscataway, NJ).

Peptide Preparation. All the peptides used in this study were prepared via a recombinant technique as described previously (*33*, *34*). The identity of the final products was verified by mass spectrometry.

NMR Measurements and Assignments. All NMR spectra were collected at 25 °C on a Bruker Avance 500 or 800 MHz spectrometer equipped with a triple-resonance pulse-field gradient probe. $^1H-^{15}N$ HSQC NMR spectra (*35*) were recorded in the States−TPPI mode for quadrature detection (*36*, *37*). All the NMR samples were prepared in the same buffer, i.e., 50 mM sodium phosphate, 50 mM NaCl, 5 mM $MgCl_2$, 0.02% NaN_3, and 95% H_2O/5% D_2O at pH 6.0. CaCdc42 samples were prepared through buffer exchange with the NMR buffer. The final concentration of GDP-loaded and GMPPNP-loaded CaCdc42 for backbone NMR assignments was 0.8 mM. Samples used for backbone assignments of labeled (^{15}N and ^{13}C or ^{15}N, ^{13}C, and ^2H) eCRIB peptides in complex with unlabeled and GMPPCP-loaded CaCdc42 were prepared by adding a slight excess of activated CaCdc42 to the labeled peptide as described previously (*33*). Backbone assignments for the aforementioned samples were obtained from the three-dimensional (3D) HNCA, HN(CO)-CA, CBCA(CO)NH, and HNCACB (optimized for C_β transfers) experiments. Free mCRIB and cCRIB peptides were prepared for NMR by dissolving the lyophilized peptides in the NMR buffer to a final peptide concentration of typically 1.2 mM. $^1H-^{15}N$ amide assignments were made from the 3D ^{15}N-edited TOCSY and 3D ^{15}N-edited NOESY experiments.

$^1H-^{15}N$ HSQC titrations were performed by stepwise addition of the nonlabeled component (at a high concentration) into the ^{15}N-labeled component (typically at a concentration of 0.1−0.3 mM) to a final 5−10-fold excess. Minimal changes in volume and pH were ensured throughout the sample preparations.

^{15}N T_1 and T_2 relaxation times and the heteronuclear NOE values were measured at 800 MHz for ^{15}N-labeled eCRIB peptides in complex with unlabeled CaCdc42 using the pulse sequences described by Farrow et al. (*38*). Relaxation delays of 2.8 s were used for the T_1 and T_2 data sets, and a 5 s recycle delay was used for the heteronuclear NOE experiment. Longitudinal relaxation delays of 10, 70 (2×), 150, 250, 320, 520 (2×), 760, 1100 (2×), 1500, 2000, and 3600 ms (where 2× represents a duplicate measurement) and T_2 delays of 14.4 (2×), 28.8, 43.2, 57.6, 72 (2×), 86.4, 100.8, 115.2 (2×), 144, and 172.8 ms were sampled for both complexes. To minimize heating between the T_2 time points, the total number of CPMG pulses was kept constant for each time point by introducing the appropriate number of dummy CPMG pulses (*39*, *40*). Steady-state heteronuclear NOE data were obtained in an interleaved manner with and without proton presaturation (3 s). All data sets were acquired with 2048 complex points in t_2 and 128 complex points in t_1.

All data sets were processed using NMRPipe (*41*). Spectral display, assignments, and analysis were performed using the NMRView software package (*42*). Time domain data were zero-filled once and apodized with a 90°-shifted cosine-squared window function. Solvent suppression was achieved by postacquisition convolution of the time domain data. Uncertainties in peak heights for R_1 and R_2 measurements were estimated from duplicate data sets. Values for R_1 and R_2 and the uncertainties were determined by nonlinear least-squares fitting of experimental data to monoexponential functions using "curvefit" (http://cpmcnet.columbia.edu/dept/gsas/biochem/labs/palmer/software/curvefit.html). Errors for the heteronuclear NOE values were estimated from the root-mean-square variation of noise in empty regions of the two spectra as described previously (*43*).

Covalent Labeling of Residue K150 in CaCdc42 R150K by the Fluorescent Probe sNBD. Residue K150 of the CaCdc42 R150K mutant was covalently modified with the fluorescent probe sNBD (Molceular Probes, Eugene, OR), essentially as described by Nomanbhoy et al. (*44*). The stoichoimetry of the fluorescent probe per protein molecule was estimated to be 1.13, based on protein concentration determined with an ϵ_{280} of 13 610 M^{-1} cm^{-1} (*45*), and using the absorbance of the sNBD moiety with an ϵ_{463} of 22 000 M^{-1} cm^{-1}.

Fluorescence Measurements. Interaction of the CRIB peptides with sNBD-labeled CaCdc42 was monitored using extrinsic fluorescence measurements (*46*) with a Hitachi F-2500 fluorescence spectrophotometer. Samples of sNBD-labeled, activated CaCdc42 were added in the assay buffer [50 mM phosphate (pH 6.8), 50 mM NaCl, and 5 mM $MgCl_2$] to a cuvette being continuously stirred. The protein concentration was 1 μM. Individual CRIB peptide dissolved in the same assay buffer was added dropwise to the cuvette. The mixture was excited at 488 nm with an excitation slit width of 5 nm. The emission spectra were scanned from 510 to 590 nm. The fluorescence emission intensity at the emission maximum of 545 nm was determined from each spectrum, and the final value was obtained by averaging the values from five scans of the same sample. Control titration experiments were performed by adding the same volume of

buffer instead of peptide. Each set of titration data was recorded three times.

Calculation of Dissociation Constants (K_d). The K_d values for the binding of the CRIB peptides to sNBD-labeled activated CaCdc42 were determined by fitting the fluorescence titration data to a simple bimolecular association model as described by Leonard et al. (*47*). The association between CaCdc42 (P) and a CRIB peptide (L) can be described by the following equation

$$P + L \underset{k_{off}}{\overset{k_{on}}{\leftrightarrow}} P{\cdot}L$$

The fluorescence intensity (F) is related to the dissociation constant (K_d) as follows

$$F = F_0 + (F_t - F_0)\left[\frac{K_d + L_T + P_T - \sqrt{(K_d + L_T + P_T)^2 - 4P_T L_T}}{2P_T}\right]$$

where F_0 and F_t are the fluorescence intensities at the starting and end points of the titration, respectively. P_T is the total concentration of sNBD-labeled activated CaCdc42, and L_T is the total concentration of the CRIB peptide at any point in the titration. Fitting of the data was carried out using Microcal (Northampton, MA) Origin 6.0. Average K_d values were determined from multiple independent measurements.

A Bivalent Dissectional Model for Interactions of the eCRIB Domain with CaCdc42. Scheme 1 depicts a two-site approximation for the interactions of Cdc42 with extended CRIB domains. The binding of one CRIB peptide fragment to one site when the other site is unoccupied is characterized by the intrinsic dissociation constants K_d. When one site is occupied, the binding of the second CRIB fragment is given by the product of K_d and the cooperativity factor $1/c_{12}$ (or $1/c_{21}$). The c_{12} and c_{21} factors provide a measure of the energetic coupling [$\Delta G_{co}^{12} = RT \ln(1/c_{12})$ or $\Delta G_{co}^{21} = RT \ln(1/c_{21})$] between the two sites. Values of c of $\neq 1$ or ΔG_{co} of $\neq 0$ indicate microscopic cooperativity, where the binding of one CRIB fragment to one site affects the affinity for the other CRIB fragment. In addition, the value of c_{12} (or c_{21}) can reveal a positive cooperativity if $c_{12} > 1$ (or $c_{21} > 1$) or a negative one if $c_{12} < 1$ (or $c_{21} < 1$). A priori, it is not clear whether the two cooperativity factors c_{12} and c_{21} would be equal or different.

When the two subfragments are covalently linked, local dissociations of the extended and apparently "bivalent" CRIB peptides exist (Scheme 1B). The overall thermodynamic dissociation constant K_d^{m-c} of the extended peptide can be written as

$$K_d^{m-c} = \frac{1}{c_{12}C_{eff}^{12}}K_d^m K_d^c = \frac{1}{c_{21}C_{eff}^{21}}K_d^m K_d^c \qquad (1)$$

where K_d^m and K_d^c are the "intrinsic dissociation constants" of the mCRIB and cCRIB peptides, respectively. C_{eff}^{12} (or C_{eff}^{21}) is an effective local concentration factor conferred by the physical linkage of two peptide fragments (*48*−*50*). The linkage Gibbs free energy is defined as $\Delta G^s = RT \ln(1/C_{eff})$ (*51*). In this context, the C_{eff} factors can be interpreted as the change in the probability of binding that results from the physical linkage of the mCRIB and cCRIB moieties in the eCRIB peptide. ΔG^s is therefore the difference between ΔG_{m-c} and the sum of ΔG_m, ΔG_c, and ΔG_{co}, where ΔG_{m-c} is the binding free energy of the eCRIB peptide for Cdc42, ΔG_m and ΔG_c are the intrinsic binding energies of mCRIB and cCRIB peptides, respectively, and ΔG_{co} is the energetic coupling between two binding sites. The bivalent binding model can therefore distinguish the cooperativity and linkage contributions of two binding subfragments through the determination of K_d^{m-c}, K_d^m, K_d^c, c_{12}, and c_{21}.

Scheme 1: A Bivalency Model for Two-Site Binding between Extended CRIB Peptides and Cdc42[a]

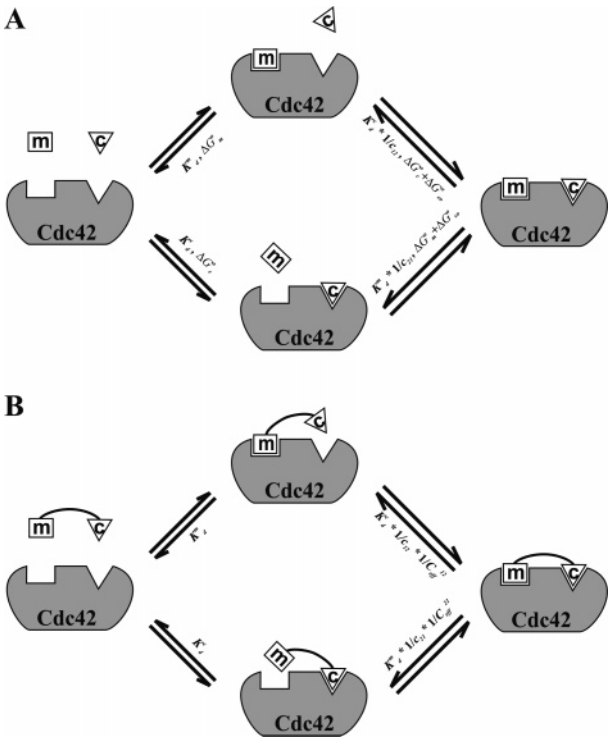

[a] (A) m and c represent the mCRIB and cCRIB fragments, respectively, as defined in Figures 2 and 3. Each dissociation constant and its corresponding Gibbs free energy are indicated according to the reaction coordinate. (B) Bivalent binding mode of covalently linked CRIB subfragments with Cdc42. The mCRIB and cCRIB sequences are assumed to have the same "intrinsic" binding affinities after linkage. An additional factor C_{eff} is introduced together with the cooperativity factors, c_{12} and c_{21} (see panel A), to define the partial dissociation constants of the individual dissociation steps. The thermodynamic dissociation constant representing complete dissociation of the extended "bivalent" CRIB peptide can be deduced following microscopic equilibria from either of the two dissociation pathways (see eq 1).

RESULTS

NMR Characterization of the CaCdc42 Protein. CaCdc42 is highly homologous to HsCdc42 except for the so-called Rho insert domain (*4*). In our study, the 13 C-terminal residues (residues 179−191) of CaCdc42 were removed to improve the protein behavior in solution required for detailed NMR experiments (*16*, *17*). Panels A and B of Figure 1 show the $^1H-^{15}N$ HSQC spectra and amide assignments of CaCdc42 bound to GDP and GMPPNP, respectively. Nearly complete assignments of the main chain $^1H^N$, ^{15}N, $^{13}C_\alpha$, and $^{13}C_\beta$ NMR signals were obtained for the two CaCdc42 complexes. Of the 178 residues in the truncated CaCdc42 protein, only 20 non-proline residues remain unassigned in

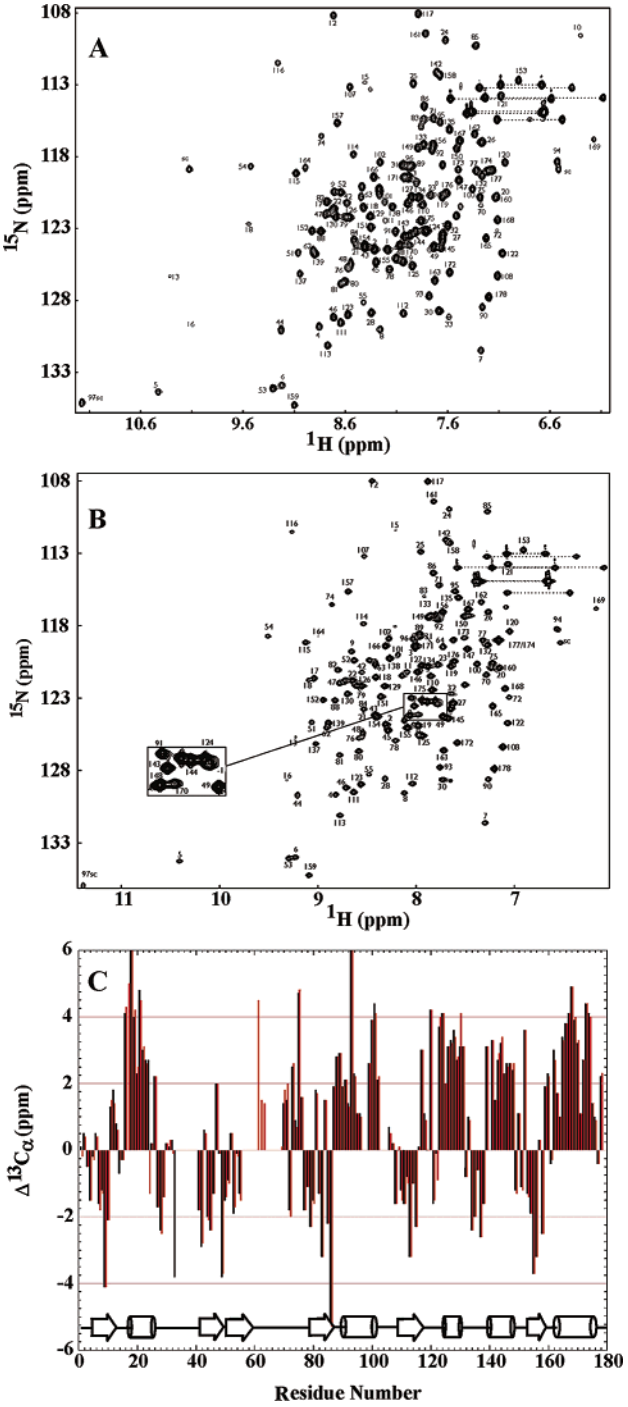

FIGURE 1: Assigned ^{1}H−^{15}N HSQC correlations and secondary structure elements of CaCdc42. Panels A and B are the ^{1}H−^{15}N HSQC spectra of CaCdc42 in the GDP-bound and GTP analogue (GMPPNP)-bound form, respectively. NMR spectra were acquired under identical conditions at 800 MHz. (C) $^{13}C_\alpha$ chemical shift deviations from the random coil values for the complexes of CaCdc42 with GDP (black) and with GMPPNP (red). A pictorial representation of the secondary structures for HsCdc42 is shown.

the CaCdc42−GDP complex, and 15 residues remain unassigned in the CaCdc42−GMPPNP complex. The increased number of assignments for activated CaCdc42 occurs in the switch regions and is an indication of decreased motional line broadening in CaCdc42 bound to the GTP analogue, as previously seen for the HsCdc42 protein (*16*, *17*). Figure 1C shows deviations of the $^{13}C_\alpha$ chemical shifts from the random coil values for CaCdc42 in both GDP and GTP forms. The secondary structure elements were deduced from these deviations over a number of consecutive amino acids (*52*). As expected from the high degree of sequence homology, the secondary structures of CaCdc42 are very similar to those of HsCdc42 (represented by the cartoon in Figure 1C) (*53*). A high level of disorder is apparent for residues 31−40 and 57−74, most of which are unassigned due to NMR line broadening and which correspond to the switch I and switch II regions of Cdc42, respectively.

NMR of the Extended CRIB Peptides from CaCla4 and Cst20 Kinase. Figure 2A compares the eCRIB sequences of the *Candida* Cla4 and Cst20 proteins with those of Cla4 and Ste20 from *S. cerevisiae* as well as that of the human PAK1 protein. The nomenclature used below for the various CRIB fragments is detailed in the legend of Figure 2A. Panels B and C of Figure 2 show the ^{1}H−^{15}N HSQC spectra and assignments for the eCRIB fragments, eCla4 and eCst20, respectively, bound to GMPPCP-loaded CaCdc42. The HSQC spectra of ^{15}N-labeled free eCRIB fragments exhibit poor resonance dispersion, indicating an unfolded conformation for these peptides in the absence of binding (*33*). The addition of unlabeled CaCdc42 in excess to ^{15}N-labeled eCRIB peptides dramatically increases the resonance dispersion of the HSQC spectra of the two eCRIBs, concomitant with essentially uniform resonance broadening. These spectra are consistent with the existence of high-affinity interactions between CaCdc42 and the eCRIB peptides (vide infra). Backbone $^{13}C_\alpha$, $^{13}C_\beta$, ^{15}N, and ^{1}H resonances of eCRIBs in complex with CaCdc42 were assigned using various heteronuclear NMR techniques. Panels D and E of Figure 2 show the secondary structure elements for the two eCRIB peptides (i.e., eCla4 and eCst20, respectively) as deduced from the positive or negative deviations of the $^{13}C_\alpha$ and $^{13}C_\beta$ chemical shift differences from random coil values (*52*). Interestingly, there are some differences in the secondary structural elements of the two closely related eCRIB peptides in complex with activated CaCdc42 in terms of both position and length. Regardless, these two eCRIBs are highly structured when bound to CaCdc42 as indicated by their HSQC NMR spectra (Figure 2B,C), though all the free CRIB peptides are highly unstructured (*33*).

Backbone Dynamics of [^{15}N]eCRIB Peptides in Complex with CaCdc42. ^{15}N relaxation data were measured at 25 °C for both ^{15}N-labeled eCRIB peptides in complex with nonlabeled CaCdc42. Figure 3A shows variation of ^{15}N−^{1}H heteronuclear NOE intensities across the eCla4 peptide in complex with CaCdc42. As indicated by the steady-state NOE values, residues C-terminal to the consensus CRIB motif have heteronuclear NOE values notably different from the N-terminal consensus sequence (i.e., mCla4). The average heteronuclear NOE value (0.61 ± 0.02) of C-terminal residues 24−38 is significantly lower than that in the N-terminal region (0.80 ± 0.02) for residues 6−21.

^{15}N relaxation data were also obtained for eCst20 in complex with CaCdc42 (Figure 3B). Overall, the heteronuclear NOE values of eCst20 in complex with CaCdc42 had a distribution similar to that of the NOE values of the eCla4−CaCdc42 complex. The average heteronuclear NOE value of the N-terminal region (0.78 ± 0.02 for residues 6−21) was close to that in eCla4. The average NOE value (0.68 ± 0.02) of C-terminal residues 24−38 is higher than the counterpart for eCla4 in complex with CaCdc42. Notably,

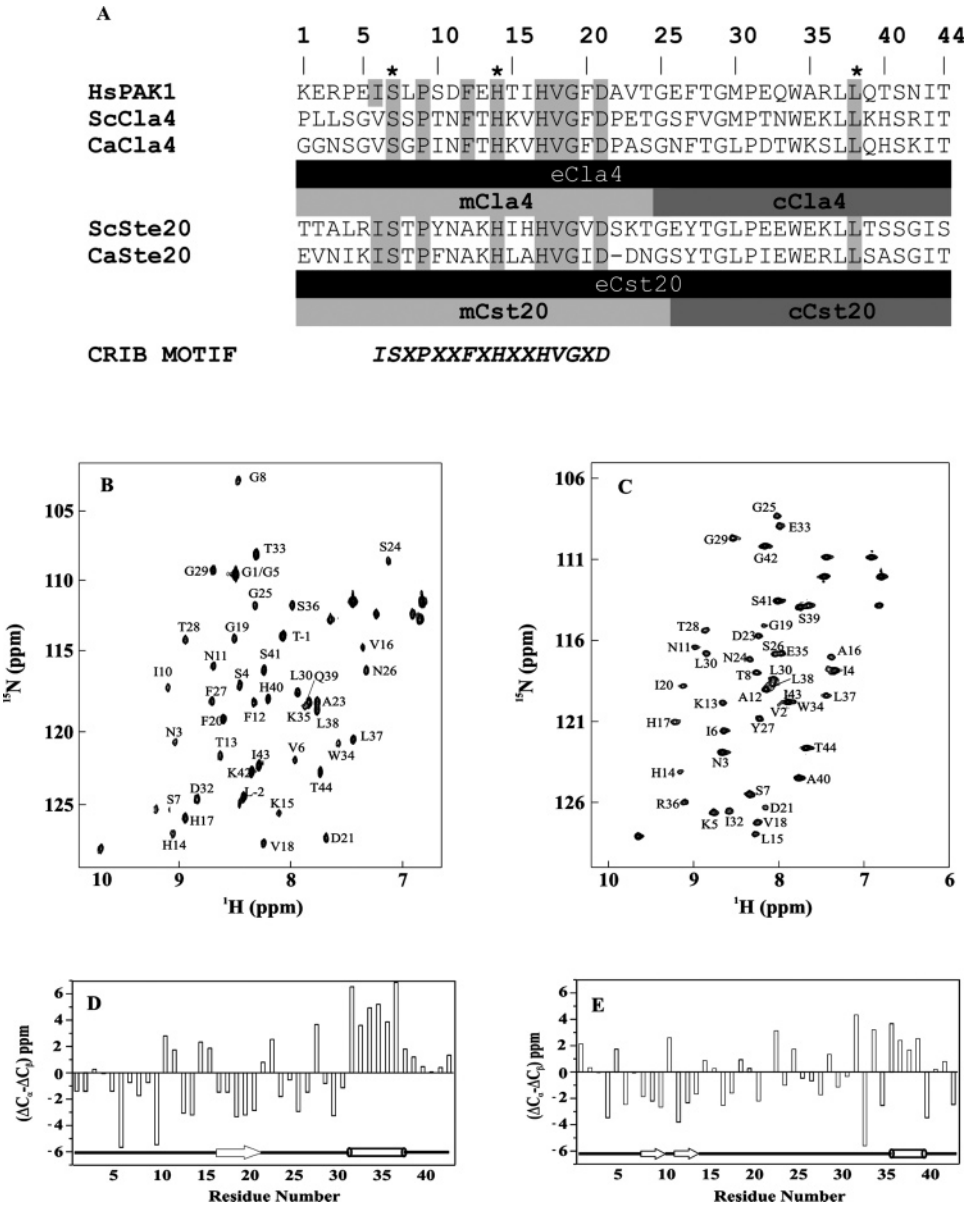

FIGURE 2: NMR characterization of the extended *Candida* CRIB domains. (A) Sequences of the Cdc42 binding domains of *Candida* Cla4 and Cst20, showing the homology to CRIB domains of human PAK1, and *Saccharomyces* Cla4 and Ste20. The extended CRIB (eCRIB) sequences comprise the consensus CRIB motif as well as 20-residue extensions to the C-terminus. In this study, the eCRIB sequences were dissected into two fragments: the minimal CRIB (mCRIB) peptides, mCla4 and mCst20, and the C-terminal CRIB (cCRIB) peptides, cCla4 and cCst20. The residues marked with asterisks were identified as being important for the activation of Ste20 kinase by ScCdc42 (*9*). (B and C) Assigned ^{1}H−^{15}N HSQC spectra of two eCRIBs in complexes with unlabeled CaCdc42 loaded with GMPPCP: (B) ^{2}H-, ^{15}N-, and ^{13}C-labeled eCla4 and (C) ^{15}N- and ^{13}C-labeled eCst20. (D and E) Secondary structure elements were deduced from the positive or negative deviations of the $^{13}C_\alpha$ and $^{13}C_\beta$ chemical shift differences over a number of consecutive amino acids for the two eCRIB peptides in complex with CaCdc42, respectively: (D) eCla4 and (E) eCst20.

three residues, i.e., Ser26, Glu35, and Arg36 (equivalent to Asn26, Lys35, and Ser36, respectively, in eCla4), are major contributing factors to the increased average NOE values of eCst20 in the C-terminal region. In all, these results strongly suggest that the motional characteristics of the different sequence segments in both high-affinity eCRIB peptides are very different when they are complexed with CaCdc42. Notably, the cCRIB segments appear to have increased mobilities on the nanosecond time scale as compared to the mCRIB segments. Similar dynamic phenomena were observed for the complex of a related CRIB peptide from human PAK3 in complex with human Cdc42 (*32*).

A detailed analysis of the ^{15}N T_1 and T_2 relaxation data is not carried out in this study, principally because the T_1 and T_2 values of the eCRIB peptides would be highly susceptible to anisotropic rotational tumbling on the basis of hydrodynamic modeling (*54*) of available Cdc42−CRIB structures. Indeed, the local correlation time (τ_{ci}) is predicted to change by as much as 2 ns due to molecular shape alone (based on Protein Data Bank entry 1E0A). Given that the actual structure of the complexes is not known, it is not possible to accurately ascertain the effects of anisotropy on the T_1 and T_2 data, which could easily be interpreted as motional effects (*54*, *55*). In comparison, the heteronuclear NOE values are virtually invariant to the effects of anisotropic tumbling and can be reliably interpreted (at least in a qualitative manner) without reference to a structure model. The local τ_c values calculated from T_1/T_2 ratios are included in the

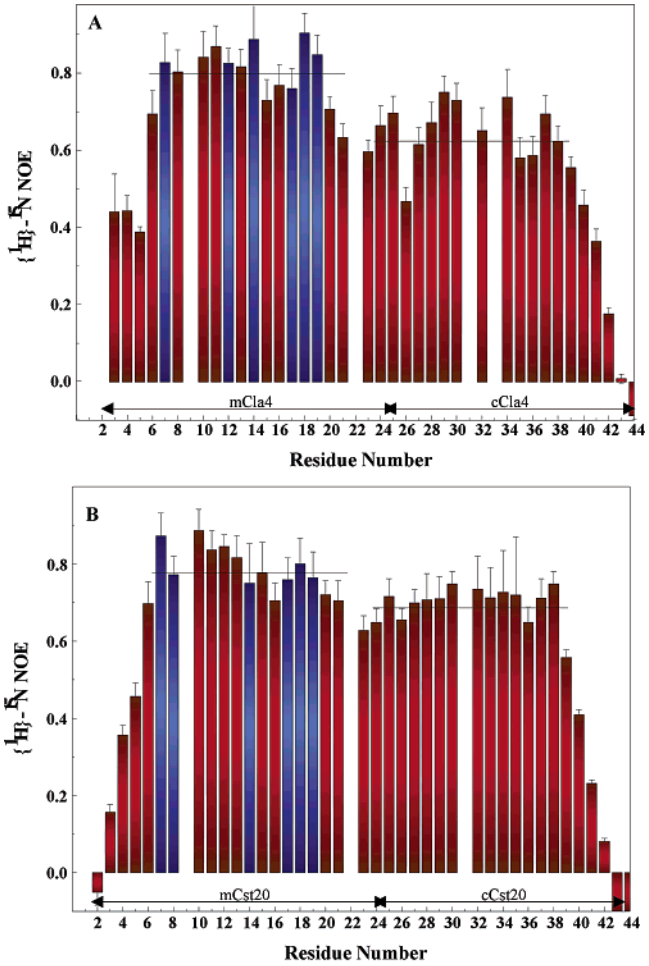

FIGURE 3: Heteronuclear $^1H-^{15}N$ NOEs of the eCRIB domains of CaCla4 and Cst20 in complex with CaCdc42: (A) [^{15}N]eCla4 and (B) [^{15}N]eCst20. The blue bars denote the consensus CRIB motif. The horizontal lines in each of the two plots indicate the average values of the steady-state NOEs for residues 6−21 and 24−38.

Supporting Information along with the predicted τ_{ci} from hydrodynamics modeling. As expected, the cCRIB regions exhibit τ_{ci} values much lower than those of the mCRIB segment, consistent with an increased level of nanosecond motions in this region. Interestingly, some of the local τ_c values for the mCRIB segments tend to be similar to predicted τ_c values from hydrodynamics calculations. This is expected if rigid structures are formed for the mCRIB region bound to CaCdc42 and the corresponding structures are similar to the NMR structure used for modeling calculations (i.e., Protein Data Bank entry 1E0A). In all, NMR relaxation data indicate that extended CRIB peptides in complex with Cdc42 have differential motional behaviors within and outside of the consensus CRIB (or mCRIB) segment. Such differential mobilities may be a consequence of microscopic and segmental dissociations of the molecular complexes as captured by the bivalent binding model shown in Scheme 1.

A Molecular Dissection of the Extended CRIB Peptides. To understand the relative contribution of the various regions of the CRIB peptides to Cdc42 binding, the eCRIB peptides were dissected into two subfragments (i.e., mCRIB and cCRIB peptides; see Figure 2 for definitions) based on their different dynamic behavior in complexes with CaCdc42 (Figure 3 and Figure S1). Binding of each CRIB peptide (i.e., eCRIB, mCRIB, and cCRIB) was followed by fluorescence and NMR titrations.

Figure 4 shows the binding isotherms obtained following the CRIB-induced changes in the sNBD fluorescence of the CaCdc42 R150K protein. All the titration curves could be best fitted to a simple bimolecular equilibrium binding model (see Experimental Procedures). In theory, fluorescence changes observed for the CaCdc42−eCRIB complexes (Figure 4A) can also reflect contributions of partial binding modes whereby either the mCRIB or cCRIB moiety occupies its binding site whereas the other moiety of the extended CRIB (i.e., eCRIB) peptide remains free (Scheme 1B). In practice, such complicating effects should be negligible for the CaCdc42−eCRIB systems. Specifically, at the low concentration ranges used for titration of the eCRIB peptides, both mCRIB and cCRIB fragments would induce insignificant changes in the fluorescence of sNBD-labeled CaCdc42 (Figure 4B,C). Even in the higher concentration range (up to 4 μM, Figure 4A), the higher bivalent affinity of the eCRIB peptides (Scheme 1B) would reduce the concentrations of the various partial binding modes to negligible levels, making it possible to determine the bivalent binding affinities, i.e., K_d^{m-c}, from the binding isotherms. The apparent K_d values thus determined for different CRIB peptides are summarized in Table 1. As expected, the eCRIB fragments exhibited the strongest affinities for CaCdc42 in the low nanomolar range. The mCRIB fragments containing the consensus CRIB sequence, ISXPXXFXHXXHVGXD (*56*), also had moderately strong binding affinities in micromolar concentrations but clearly, as seen previously for the human PAK homologues (*7*, *8*), require extra residues to achieve stronger binding to Cdc42. The cCRIB peptides exhibited much weaker affinities for the CaCdc42 protein. The K_d value of cCla4 for binding to CaCdc42 is in the high micromolar range (275 μM). An even weaker binding (K_d = 1160 μM) was observed between cCst20 and CaCdc42 with the current fluorescence titration strategy.

These results are substantiated by NMR titrations of unlabeled CaCdc42 into the ^{15}N-labeled mCRIB and cCRIB fragments (Figure 5; see the legend for more details). Widespread NMR line broadening was observed for both mCRIB fragments (Figure 5A for mCla4 and Figure 5D for mCst20), indicating a relatively fast to intermediate rate of dissociation of the Cdc42−peptide complexes. We noted attenuation of resonance peaks for [^{15}N]mCst20, which may reflect the tighter binding observed for this complex by fluorescence titrations over the mCla4−CaCdc42 complex (vide supra). As expected, titration of CaCdc42 also had very different effects on the NMR signals of the cCRIB peptides. Most of the $^1H-^{15}N$ HSQC resonance peaks of cCla4 were shifted by the titration of CaCdc42 (Figure 5B), whereas the resonance peaks of [^{15}N]cCst20 remained relatively unaffected by CaCdc42 titration (Figure 5E). Again, these results are consistent with the observed affinities for Cdc42 determined from fluorescence titrations (Table 1).

A striking difference between the Cla4 and Cst20 systems was observed when unlabeled mCRIB peptides were titrated into the ^{15}N-labeled cCRIB peptides preincubated with an excess (10-fold) of CaCdc42 (Figure 5C,F). The [^{15}N]cCla4 resonances were unaffected by further additions of mCla4. Surprisingly, the [^{15}N]cCst20 resonances were dramatically

Table 1: Dissociation Constants for Binding of *Candida* CRIB Fragments to CaCdc42 Measured by NMR and Fluorescence Titrations

	mCla4 (K_d^m)[a] (μM)	mCst20 (K_d^c) (μM)	mCla4 (+cCla4) (K_d^m/c_{21})[b] (μM)	mCst20 (+cSt20) (K_d^m/c_{21}) (μM)	cCla4 (K_d^c) (μM)	cCst20 (K_d^c) (μM)	cCla4 (+mCla4) (K_d^c/c_{12}) (μM)	cCst20 (+mCst20) (K_d^c/c_{12}) (μM)	eCla4 (K_d^{m-c}) (μM)	eCst20 (K_d^{m-c}) (μM)	mCst20/ cCst20[c]
NMR[d]	+	+	+	+++	+	−	+	+	+++++	+++++	−
FLU	4.2 ± 0.15	0.43 ± 0.03	4.1 ± 0.13	0.081 ± 0.002	275 ± 9	1160 ± 106	311 ± 12	207 ± 10	0.025 ± 0.002	0.046 ± 0.002	ND[e]

[a] All the dissociation constants are treated as the apparent values illustrated in Scheme 1. [b] c_{12} and c_{21} are the cooperativity factors, as defined in Scheme 1. [c] The control binding experiment in the absence of CaCdc42 protein. [d] ^{15}N NMR HSQC titration experiments: +++++, slow-dissociating complexes; +++, fast-dissociating complex with a K_d of <1 μM; +, fast-dissociating complex with a K_d of >1 μM; −, no significant binding. [e] Not determined.

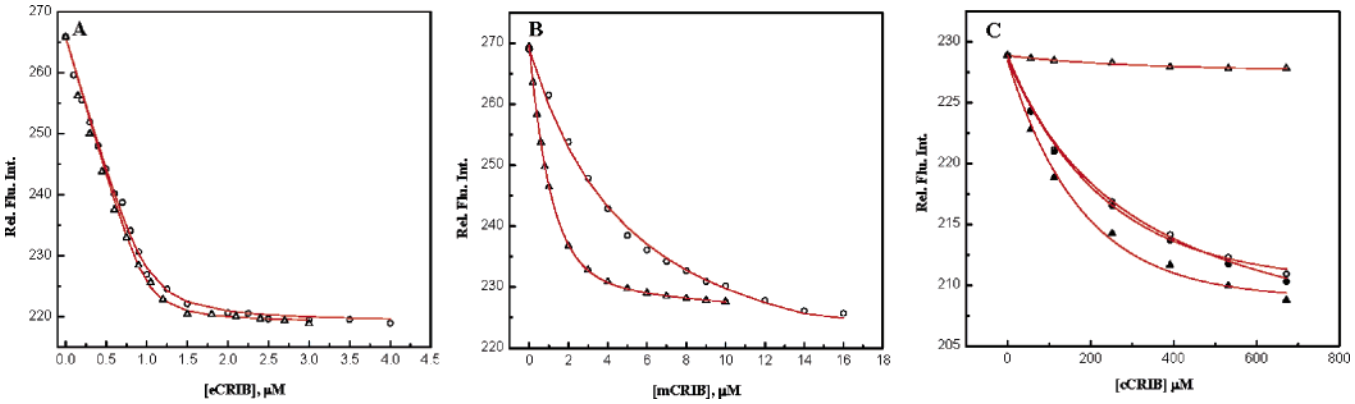

FIGURE 4: Fluorescence titration of sNBD-labeled, GMPPCP-loaded CaCdc42 (R150K) with different CRIB peptides. Experiments were carried out as described in Experimental Procedures. sNBD-labeled and GMPPCP-loaded CaCdc42 R150K (1 μM) was titrated with the indicated amounts of different CRIB fragments shown in Figure 2: (A) eCla4 (○) and eCst20 (△), (B) mCla4 (○) and mCst20 (△), and (C) cCla4 (○), cCst20 (△), cCla4 in the presence of mCla4 (●), and cCst20 in the presence of mCst20 (▲). Solid lines represent fits of the data to a bimolecular association model as described in Experimental Procedures.

affected upon titrations of the mCst20 peptide. Thus, there appears to be a cross-talk between the mCRIB and cCRIB peptides in the Cst20 system and not in the Cla4 system. The same results were seen when unlabeled cCRIB peptides were titrated into [^{15}N]mCRIB peptides preincubated with CaCdc42. Namely, the mCla4 exhibited no obvious changes in NMR signals, whereas the mCst20 was further broadened by titrations of the cognate peptides (data not shown).

Fluorescence measurements were used to substantiate and quantify the effects of these cross-titrations (Table 1). In agreement with NMR data, the affinity of the Cla4 peptide fragments for CaCdc42 was not significantly affected by the addition of the cognate peptide. In contrast, the affinities of the Cst20 peptide fragments preincubated with CaCdc42 exhibited a dramatic enhancement in binding for CaCdc42 by ~5.5-fold, upon addition of the cognate Cst20 peptide (Table 1). Thus, upon addition of mCst20 to the cCst20−CaCdc42 complex, the affinity of cCst20 for CaCdc42 increased from a K_d of 1160 μM to a K_d of 207 μM (Table 1 and Figure 3C). Similarly, mCst20 affinity for CaCdc42 increased from 0.43 to 0.081 μM when cCst20 was added to a preincubated mCst20−CaCdc42 complex. These results strongly suggest that the eCst20 and eCla4 peptides exhibit different mechanisms for binding CaCdc42, in which the long eCst20 peptide utilizes a cooperative mechanism for high-affinity interaction while eCla4 does not. In addition, NMR titration showed that the cCst20 and mCst20 peptides had no affinity for each other in the absence of CaCdc42 (Table 1).

Mapping of the Binding Surfaces of the mCRIB and cCRIB Fragments on CaCdc42. The binding surfaces on CaCdc42 for the mCla4, mCst20, and cCla4 peptides were identified by monitoring complexation-induced perturbations of the ^{1}H−^{15}N HSQC resonances of CaCdc42 (Figure 6). The two mCRIBs perturb a similar region on CaCdc42, namely, resonances around the switch I region of most residues from residue 10 to 55. Residues in the switch II region and in C-terminal helix α5 were also affected. Resonance perturbations caused by the two mCRIBs are also similar to those identified for binding of the PAK2 mCRIB to human Cdc42 (*57*). The magnitude of the binding-induced perturbations on CaCdc42 is much greater for mCst20 (Figure 6B) than for mCla4 binding (Figure 6A). This observation may be related to a stronger binding affinity of mCst20 for CaCdc42 determined by the fluorescence binding assay (Table 1). The mCst20 binding also significantly perturbs additional resonances for the residues located on switch II, β4, β5, and α5 (Figure 6B) as compared to mCla4 (Figure 6A).

Although the cCla4 peptide binds only weakly to CaCdc42, the binding interactions caused resonance perturbations in the ^{1}H−^{15}N HSQC spectrum of CaCdc42 (Figure 6C). The magnitude of the binding-induced perturbations on CaCdc42 is much smaller for cCla4 than for mCla4 binding. However, the CaCdc42 surface expected to be most perturbed by cCla4 could not be delineated since NMR signals from these regions of CaCdc42 are very broad, and therefore cannot be assigned in activated CaCdc42. As expected, the cCst20 peptide did not cause observable perturbations to CaCdc42 resonances (data not shown).

DISCUSSION

The concept of modular protein−protein interactions has provided the molecular basis for our understanding of many

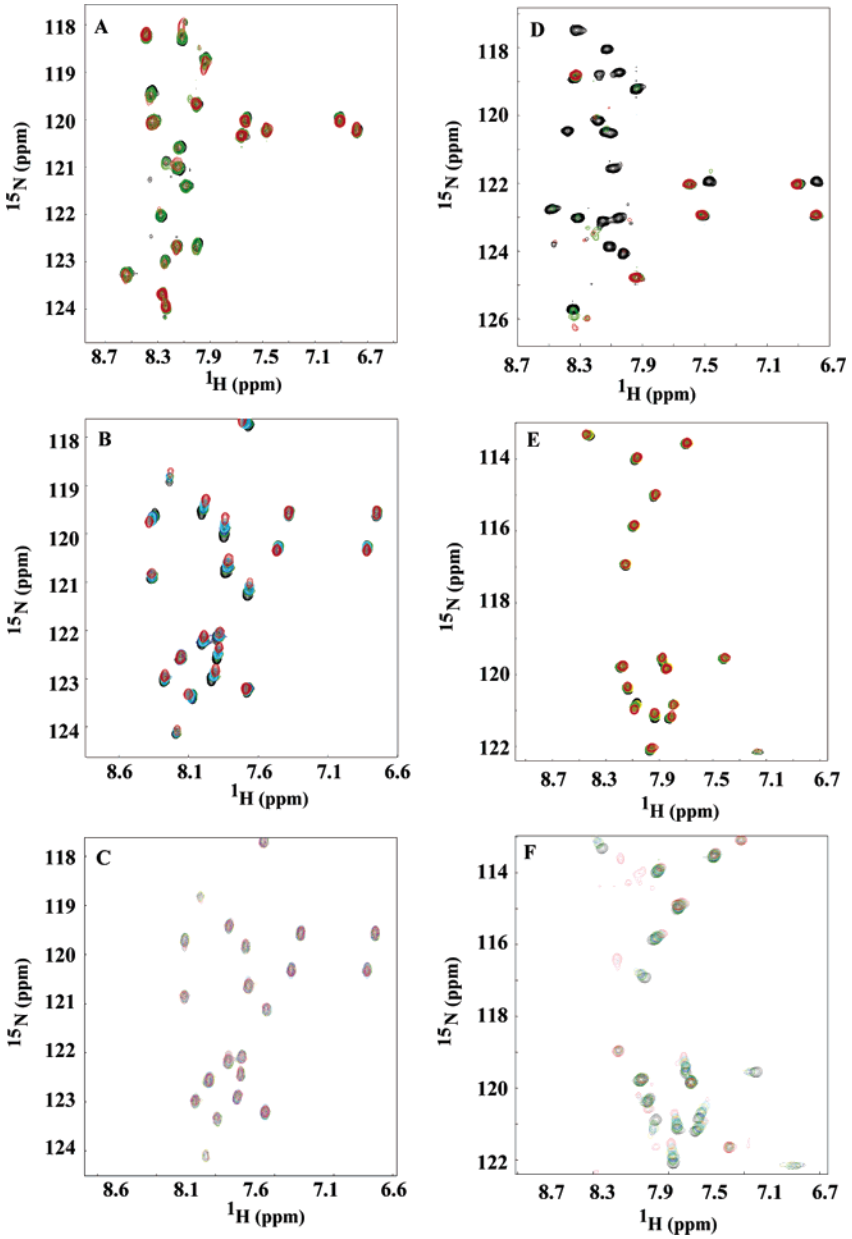

FIGURE 5: Resonance perturbations in the ^{1}H−^{15}N HSQC spectra of the CRIB peptides induced by CaCdc42: (A) [^{15}N]mCla4, (B) [^{15}N]-cCla4, (C) [^{15}N]cCla4 in the presence of mCla4, (D) [^{15}N]mCst20, (E) [^{15}N]cCst20, and (F) [^{15}N]cCst20 in the presence of mCst20. Identical CaCdc42 and peptide concentrations were used in all titration experiments. Spectra are colored from black (free peptide) to red (CaCdc42 in 10-fold excess). Differential binding properties for the different CRIB fragments are clearly seen, in exact agreement with fluorescence titrations (Table 1).

biological and cell signaling pathways (*23*). As such, a multivalent, combinatorial, and dynamic perspective has recently come into focus as a general framework for representing the physical nature of protein−protein complexes and their roles in regulating biological functions (*21*, *23*, *58*). Of a plethora of such protein−protein complexes, we focus on the Cdc42 protein and its interactions with the CRIB polypeptides contained by many intracellular proteins (*59*) which control different signaling cascades and ultimate fates of the cell. One particular characteristic of the Cdc42−CRIB complexes is the very large surface area of binding encompassing much of the extended CRIB sequence (*12*−*14*, *16*−*18*) as compared to related cell-signaling protein complexes (*60*). In addition, high-affinity polypeptides containing the CRIB motif are predominantly unfolded before binding in contrast to other protein functional domains (*7*, *33*, *60*). As a consequence, the thermodynamics of binding may become unpredictably complex as a result of possible coupling between peptide folding and Cdc42 binding (*60*). On the other hand, the extended molecular interfaces seen in these Cdc42−CRIB complexes may be viewed as the multivalency effect (*61*, *62*) manifested by cell signaling protein−protein interactions (*21*, *23*, *58*, *59*). In such systems, high-affinity binding is achieved via multiple binding sites, each of which alone may be weak. However, when linked together, the binding energies may add and the affinities may multiply (*51*, *62*). As well, multivalent molecular binding naturally spans large contact surface areas as seen from the structural perspective and incurs no prerequisites for peptide folding before complexation (*62*).

The multivalent framework of molecular interactions has the same origin as the widely used additivity relationships

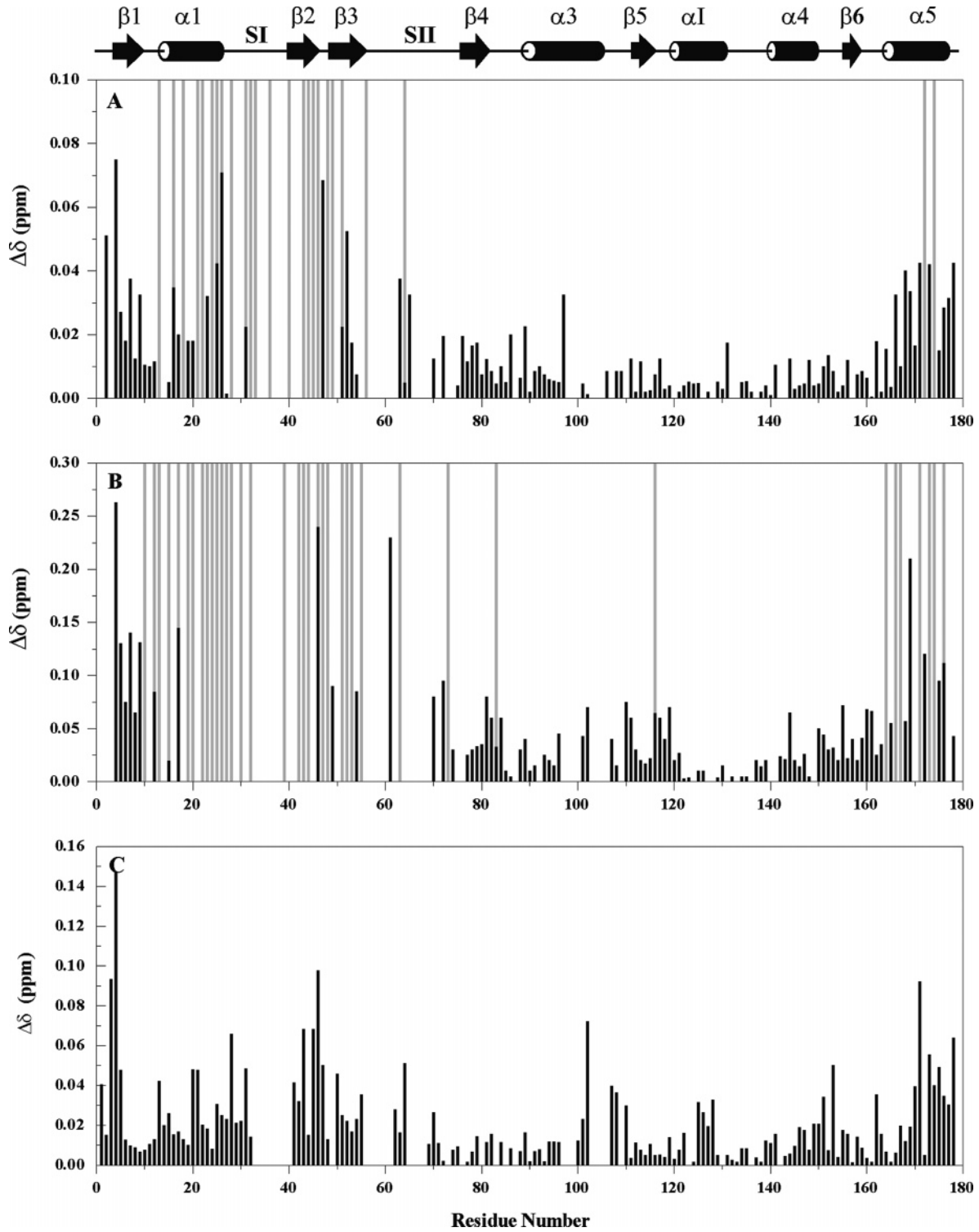

FIGURE 6: Summary of the resonance perturbations in the $^{1}H-^{15}N$HSQC spectra of GMPPCP-bound CaCdc42 induced by the binding of the various CRIB fragments. Resonance shifts are reported as a weighted vector sum of the ^{1}H and ^{15}N deviations. The vector sum (Sum) is expressed in the equation $\text{Sum} = (CS_{^{1}H}^{2} + CS_{^{15}N}^{2})^{1/2}$, where $CS_{^{1}H}$ and $CS_{^{15}N}$ are chemical shifts of each resonance along with ^{1}H and ^{15}N coordination, respectively: (A) by mCla4, (B) by mCst20, and (C) by cCla4. Gray bars denote CaCdc42 residues exhibiting significant broadening upon peptide binding.

of binding free energies (*50*, *51*, *62*−*64*). The latter descriptions, however, become very complex for highly cooperative molecular interactions (*62*, *63*), especially when the overall binding free energy is on the same order of magnitude as that of the constituent moieties. In other words, the observed binding free energies are often very small (*65*) and are results from subtracting apparently very large numbers attributed to the intrinsic free energies of "binding" constituents (*51*, *65*). The new multivalent perspective (*48*−*50*, *64*) expands on the binding behaviors of multidomain proteins relative to their functional subfragments (*51*, *66*). In particular, the redefined multivalent framework uses as binding constituents only those that have experimentally observable, often weak, binding affinities (*48*−*50*, *62*, *64*). It then treats affinity

Table 2: Gibbs Free Energies, Cooperativity Factors, and Effective Concentrations for Site-Specific Binding of *Candida* CRIB Fragments to CaCdc42[a]

	$\Delta G^{obs}_{m,1}$ (kcal/mol)	$\Delta G^{obs}_{c,1}$ (kcal/mol)	$\Delta G^{obs}_{m,2}$ (kcal/mol)	$\Delta G^{obs}_{c,2}$ (kcal/mol)	ΔG^{obs}_{m-c} (kcal/mol)	ΔG_{co} (kcal/mol)	ΔG^{s} (kcal/mol)	c_{12}	c_{21}	C_{eff} (mM)
eCla4	−7.33	−4.86	−7.35	−4.78	−10.36	≅0	1.77	0.88	1.02	51.0
eCst20	−8.68	−4.00	−9.67	−5.02	−10.00	−1.00	3.68	5.60	5.31	2.0

[a] All the free energy values are treated as the apparent values calculated with the equation $\Delta G^{\circ} = RT \ln K_d$, $RT \ln(1/c_{12})$, or $RT \ln(1/C_{eff})$, where the standard state is defined as 1 M and R is the gas constant (1.9872 cal mol^{-1} K^{-1}) at 298 K.

enhancement of the overall molecule as the combined effects of individual binding with the statistical advantages of linking in the form of increased local (or effective) concentrations (*48*−*50*, *64*). Such purely "statistical" or avidity advantages can also be coupled with perturbations of individual binding affinities of the linked constituents caused either by the linker chemistry or by (positive or negative) cooperativity effects (*62*). This multivalent formulation is best illustrated using the simplest case of bivalent binding as shown in Scheme 1, where the statistical or avidity factor has been separated from cooperativity effects. Integrated analysis using the multivalent−bivalent model must then require the experimental determination of all possible binding constants, i.e., those of the conjugated molecule and the constituent binding moieties.

Following previous observations with the human Cdc42−PAK system (*32*), our NMR relaxation data show that extended CRIB peptides derived from two fungal kinases, i.e., the *Candida* Cla4 and Cst20 proteins, again exhibit differential mobilities in complex with *Candida* Cdc42 when comparing the CRIB consensus region with the affinity-enhancing C-terminal extension (Figure 3). The higher structural order of the consensus CRIB region is strongly correlated with the higher affinities of peptide fragments encompassing the CRIB motif, i.e., the mCRIB peptides (Figure 2A and Table 1). Very interestingly, we found that cCRIB peptides representing the extensions C-terminal to the CRIB region uniformly have very weak binding affinities in the millimolar to sub-millimolar range (Table 1). These low affinities of binding appear to be related to the decreased structure order or increased structure mobility of this region of the extended CRIB peptides in complex with CaCdc42 (Figure 3). Overall, the highly conserved mCRIB fragments contribute to the majority of binding for CaCdc42, with affinities in the low micromolar range, whereas the weaker-binding cCRIB fragments exhibited higher sequence diversity among the different eCRIB sequences. Such binding characteristics have also been observed in other high-affinity protein−protein interactions of structurally homologous protein families, e.g., T-cell receptors, peptide-bound MHC complexes (*67*), and the colicin−immunity protein complexes (*68*). For the best-characterized colicin−immunity system, an alanine scan revealed a binding "hot spot" common to all the immunity proteins and accounting for two-thirds of the binding energy. The more variable region, however, contributed much less to the overall affinity, but was shown to be critical for the exquisite specificity displayed in these complexes, a phenomenon termed dual recognition (*69*−*71*). More importantly, tremendous affinity enhancement conferred by such a dual recognition appears to follow the bivalent model of binding (*72*), as described previously for both two-domain proteins (*51*, *66*) as well as for divalent ligands (*48*). In a similar vein, the conserved, relatively high-affinity mCRIB sequences generally bind the same region of Cdc42, whereas structural diversity is demonstrated by the more variant C-terminal sequence segments. Such binding may be ubiquitous to the PAK family of kinases containing CRIB domains, since similar motional characteristics have been reported for a human Cdc42−CRIB complex (*32*).

Quantitative data for binding of the two extended *Candida* CRIB peptides to CaCdc42 (Table 2) revealed that a positive cooperativity exists between the two CRIB fragments of eCst20 ($c_{12} = 5.6$, $c_{21} = 5.3$, $\Delta G_{co} \cong -1.00$ kcal/mol), while the two fragments of eCla4 lack any significant cooperative effects between the two dissected peptide segments ($c_{12} \sim c_{21} \cong 1$, $\Delta G_{co} \cong 0$ kcal/mol). Very significantly, there is an apparent symmetry in the allosteric effects between the binding of the two cognate CRIB peptide fragments. In other words, we found that the two separate peptide fragments either do not influence each other in their binding to Cdc42, as seen for eCla4, or enhance each other's binding affinity to a similar degree, i.e., $c_{12} \sim c_{21} = 5.5$ for eCst20 peptides (Tables 1 and 2). A previous study also reported weaker binding affinities in the sub-micromolar range ($K_d \sim 0.5\ \mu$M) for a peptide fragment containing the consensus CRIB motif of human WASP as well as for a longer CRIB peptide containing only part of the C-terminal extensions (*7*). Only a fully extended peptide containing the entire eCRIB sequence was found to restore the high-affinity characteristics of the full-length effector protein (*7*). Very similar binding behaviors were observed for truncated fragments of the CRIB domain-containing peptides derived from the PAK proteins (*8*, *31*). All these observations taken together suggest that binding affinities determined by use of the separated peptides, i.e., those for mCRIB and cCRIB fragments, correspond with a high degree of accuracy to those of the same sequences within the extended (or linked) peptides, as shown in Scheme 1B. In addition, the two extended CRIB peptides from *Candida* kinases can be modeled as bivalent molecules with well-defined C_{eff} parameters, given the symmetric cooperative binding behavior of the dissected subfragment peptides (i.e., $c_{12} \sim c_{21}$; Table 1). As such, the bivalent binding model (Scheme 1B) may represent a molecular mechanism of binding for the Cdc42−CRIB interaction system, which is also supported experimentally by truncation analyses, by three-dimensional structures of known Cdc42−CRIB complexes, by heteronuclear NMR relaxation (NOE) experiments (Figure 3), and by the weak-binding behaviors of the dissected subfragments.

Overall, linkage of the two individual CRIB subfragments does not result in binding free energies as expected in a simple additive mode. The differences in the binding free energy (ΔG^{s}) between the extended CRIB peptides and the sum of the binding free energies of the two fragments are 1.77 kcal/mol for eCla4 and 3.68 kcal/mol for the eCst20 sequence (Table 2). Interpreted using the bivalent binding

model (Scheme 1) for the conjugated peptides (i.e., eCRIBs), the eCla4 peptide appears to have an enhanced bivalency with a C_{eff} of 51 mM after covalent linkage. Such a value of effective concentrations falls well within the range of those observed for affinity enhancement within many bivalent−multivalent systems (*50*). On the contrary, the eCst20 peptide has a rather weak linkage effect with a smaller C_{eff} value of 2.0 mM, indicating that the high-affinity binding of eCst20 arises in addition from the observed cooperative effects between the two binding moieties. Therefore, high-affinity binding of the full-length CRIB peptides can be effected by the linkage (i.e., via the avidity effect) as well as by cooperative contributions of two individually weak constituent binding sequences. By comparison, the linked sequence in eCst20 appears to be less favorable than that of eCla4 given that a 25-fold higher effective local concentration can be achieved by linking the two relatively independent segments in the eCla4 peptide. In all, covalent linkage of weaker binding peptides can achieve dramatically increased binding affinities (*61*) either through purely statistical (avidity) effects, as witnessed for eCla4, or in combination with allostery (*62*), as demonstrated with eCst20. Such subtleties in binding mechanism have not been reported for the Cdc42−CRIB interaction and are unlikely to be identified from structural data of protein−protein complexes alone. NMR relaxation measurements for two fungal CRIB domains (Figure 3) coupled with a bivalent dissectional analysis detailed in the current study further identify stepwise dissociations, i.e., the bivalent binding model of Scheme 1, as a highly plausible mechanism of molecular interactions occurring in Cd42−CRIB complexes. As such, this bivalent binding model can also explain the observed lower binding affinities (i.e., 20−50 nM) instead of being much stronger given the large contact surfaces engaged for Cdc42−effector interactions (*60*). Such highly dynamic molecular interactions have distinct advantages of being more easily reversible (*51*, *62*) as required for the regulation of biological signaling networks.

So far, detailed structural information about the interface between the two eCRIB peptides and CaCdc42 is not yet available. However, HSQC perturbation experiments (Figure 6) have shown that both mCla4 and mCst20 significantly perturbed the resonances in the switch I region of CaCdc42 composed of β1, α1, S1, β2, β3, and α5. The cross-titration results (Figure 5C,F) with cognate fragments highly suggest that the two cCRIB peptides have very different interaction interfaces with CaCdc42, despite the sequence similarity of both peptides to the PAK1 eCRIB domain. This is also indicated by the chemical shifts of the eCRIB fragments in complex with CaCdc42, which show some differences in secondary structure (Figure 1). It is known that the cCRIB segments interact with human Cdc42 in at least two different structural modes, which can be represented by one Cdc42/PAK−CRIB complex (*16*) and the Cdc42/ACK−CRIB structure (*17*) and a second Cdc42/PAK−CRIB complex (*18*), respectively. One possibility is that the eCst20 peptide may adopt a WASP-like structure (*14*), since contacts between the mCRIB and cCRIB fragments observed in this structure may be important for a cooperative mechanism. In such a structure, the dissection point leading to the mCst20 and cCst20 fragments would correspond to the turn region of a putative β-hairpin, which is observed in the three-dimensional structures of the extended CRIB domains from both WASP (*14*) and a PAK protein (*16*). However, we note that no interaction between the mCst20 and cCst20 peptides in the absence of CaCdc42 could be observed by NMR titration. Given that the mCRIB portions (i.e., the consensus CRIB motif) contribute predominantly to the energy of binding of eCRIB peptides to CaCdc42, one would expect that the cCRIB sequences contribute not only to the enhancement of the binding affinity (in either avidity or allosteric energetics) but also to the specificity of the eCRIB peptides from various protein kinases as well. The different energetic contributions of the cCRIB fragments from the CaCla4 and Cst20 protein kinases may assume individual functional roles in the activation of these protein kinases.

The genetic and mutation assays revealed that the eCRIB domain of Ste20 interacts with Cdc42 primarily via mCRIB, especially residues Ser7 and His14 (Figure 2), and with the Ste20 kinase domain via the cCRIB segment (e.g., residue Leu38). The Cdc42−mCRIB interaction appears to antagonize the autoinhibitory effect of the latter (cCRIB−kinase) interaction (*9*). Our current results show that the mCRIB fragment of Cst20 (i.e., mCst20) alone is only ∼10-fold less active than the full-length eCRIB (Table 1) and that the cCst20 peptide has much weaker binding to CaCdc42, suggesting that the CaCdc42−mCst20 interaction alone may be strong enough to activate the Cst20 kinase. Indeed, in vivo functional studies indicated that mutations of the corresponding cCRIB segment of *S. cerevisiae* Ste20 (for example, Leu38Gly) did not significantly affect its binding to Cdc42 (*9*). On the other hand, the mCRIB segment of CaCla4 (i.e., mCla4) is 10-fold less active than mCst20 (Table 1), suggesting that the mCla4−Cdc42 interaction alone may not be strong enough to activate the CaCla4 kinase. Additional contributions from the cCla4 sequence are needed to enhance the Cla4−Cdc42 interaction. Surprisingly, residue Phe12 in the CRIB consensus (Figure 2), which has crucial contacts with human Cdc42 in the Cdc42−CRIB structures (*16*, *18*), is replaced with Ala12 in the Cst20 CRIB, and this alteration appears to increase the binding affinity of mCst20 for CaCdc42.

The previous two-hybrid assays also found that mutations of two histidines in the CRIB motif of Ste20 blocked the association of the kinase with CaCdc42 and the loss of association was correlated with a loss of biological function (*73*). This finding again shows that signaling by wild-type Ste20 requires that its kinase activity be stimulated by Cdc42 (*9*, *73*). On the other hand, the Cla4 kinase from *S. cerevisiae* showed weak stimulation of its activity by Cdc42 compared to other members of the PAK family in vivo (*74*). Therefore, binding of the different eCRIB peptides to CaCdc42 may have distinct mechanisms as we have observed through our bivalent dissectional analyses. Functional data coupled with biophysical studies therefore provide a clear rationale for further analyses of the interactions of two closely related CRIB peptides from the same fungal organism. Together with the bivalency model established in this study, it may become possible to design and discover novel antifungal agents targeting the specific features of the otherwise ubiquitous CRIB−Cdc42 interaction both in yeast and in mammalian cells.

SUPPORTING INFORMATION AVAILABLE

Local correlation times (τ_{ci}) of eCla4 and eSte20. This material is available free of charge via the Internet at http://pubs.acs.org.

REFERENCES

1. Cotteret, S., and Chernoff, J. (2002) The evolutionary history of effectors downstream of Cdc42 and Rac, *Genome Biol. 3*, 1−7.
2. Erickson, J. W., and Cerione, R. A. (2001) Multiple roles for Cdc42 in cell regulation, *Curr. Opin. Cell Biol. 13*, 153−157.
3. Hall, A. (1998) Rho GTPases and the actin cytoskeleton, *Science 279*, 509−514.
4. Johnson, D. I. (1999) Cdc42: An essential Rho-type GTPase controlling eukaryotic cell polarity, *Microbiol. Mol. Biol. Rev. 63*, 54−105.
5. Bishop, A. L., and Hall, A. (2000) Rho GTPases and their effector proteins, *Biochem. J. 348*, 241−255.
6. Pirone, D. M., Carter, D. E., and Burbelo, P. D. (2001) Evolutionary expansion of CRIB-containing Cdc42 effector proteins, *Trends Genet. 17*, 370−373.
7. Rudolph, M. G., Bayer, P., Abo, A., Kuhlmann, J., Vetter, I. R., and Wittinghofer, A. (1998) The Cdc42/Rac interactive binding region motif of the Wiskott Aldrich syndrome protein (WASP) is necessary but not sufficient for tight binding to Cdc42 and structure formation, *J. Biol. Chem. 273*, 18067−18076.
8. Thompson, G., Owen, D., Chalk, P. A., and Lowe, P. N. (1998) Delineation of the Cdc42/Rac-binding domain of p21-activated kinase, *Biochemistry 37*, 7885−7891.
9. Lamson, R. E., Winters, M. J., and Pryciak, P. M. (2002) Cdc42 regulation of kinase activity and signaling by the yeast p21-activated kinase Ste20, *Mol. Cell. Biol. 22*, 2939−2951.
10. Lei, M., Lu, W., Meng, W., Parrini, M. C., Eck, M. J., Mayer, B. J., and Harrison, S. C. (2000) Structure of PAK1 in an autoinhibited conformation reveals a multistage activation switch, *Cell 102*, 387−397.
11. Manser, E., Leung, T., Salihuddin, H., Tan, L., and Lim, L. (1993) A non-receptor tyrosine kinase that inhibits the GTPase activity of p21cdc42, *Nature 363*, 364−367.
12. Daniels, R. H., and Bokoch, G. M. (1999) p21-activated protein kinase: A crucial component of morphological signaling? *Trends Biochem. Sci. 24*, 350−355.
13. Hoffman, G. R., and Cerione, R. A. (2000) Flipping the switch: The structural basis for signaling through the CRIB motif, *Cell 102*, 403−406.
14. Abdul-Manan, N., Aghazadeh, B., Liu, G. A., Majumdar, A., Ouerfelli, O., Siminovitch, K. A., and Rosen, M. K. (1999) Structure of Cdc42 in complex with the GTPase-binding domain of the 'Wiskott-Aldrich syndrome' protein, *Nature 399*, 379−383.
15. Garrard, S. M., Capaldo, C. T., Gao, L., Rosen, M. K., Macara, I. G., and Tomchick, D. R. (2003) Structure of Cdc42 in a complex with the GTPase-binding domain of the cell polarity protein, Par6, *EMBO J. 22*, 1125−1133.
16. Morreale, A., Venkatesan, M., Mott, H. R., Owen, D., Nietlispach, D., Lowe, P. N., and Laue, E. D. (2000) Structure of Cdc42 bound to the GTPase binding domain of PAK, *Nat. Struct. Biol. 7*, 384−388.
17. Mott, H. R., Owen, D., Nietlispach, D., Lowe, P. N., Manser, E., Lim, L., and Laue, E. D. (1999) Structure of the small G protein Cdc42 bound to the GTPase-binding domain of ACK, *Nature 399*, 384−388.
18. Gizachew, D., Guo, W., Chohan, K. K., Sutcliffe, M. J., and Oswald, R. E. (2000) Structure of the complex of Cdc42Hs with a peptide derived from P-21 activated kinase, *Biochemistry 39*, 3963−3971.
19. Owen, D., Mott, H. R., Laue, E. D., and Lowe, P. N. (2000) Residues in Cdc42 that specify binding to individual CRIB effector proteins, *Biochemistry 39*, 1243−1250.
20. Dyson, H. J., and Wright, P. E. (2002) Coupling of folding and binding for unstructured proteins, *Curr. Opin. Struct. Biol. 12*, 54−60.
21. Ptashne, M., and Gann, A. (2003) Signal transduction. Imposing specificity on kinases, *Science 299*, 1025−1027.
22. Drews, J. (2000) Drug discovery: A historical perspective, *Science 287*, 1960−1964.
23. Pawson, T., and Nash, P. (2003) Assembly of cell regulatory systems through protein interaction domains, *Science 300*, 445−452.
24. Leberer, E., Harcus, D., Broadbent, I. D., Clark, K. L., Dignard, D., Ziegelbauer, K., Schmidt, A., Gow, N. A., Brown, A. J., and Thomas, D. Y. (1996) Signal transduction through homologs of the Ste20p and Ste7p protein kinases can trigger hyphal formation in the pathogenic fungus *Candida albicans*, *Proc. Natl. Acad. Sci. U.S.A. 93*, 13217−13222.
25. Leberer, E., Ziegelbauer, K., Schmidt, A., Harcus, D., Dignard, D., Ash, J., Johnson, L., and Thomas, D. Y. (1997) Virulence and hyphal formation of *Candida albicans* require the Ste20p-like protein kinase CaCla4p, *Curr. Biol. 7*, 539−546.
26. Ramer, S. W., and Davis, R. W. (1993) A dominant truncation allele identifies a gene, STE20, that encodes a putative protein kinase necessary for mating in *Saccharomyces cerevisiae*, *Proc. Natl. Acad. Sci. U.S.A. 90*, 452−456.
27. Leberer, E., Dignard, D., Harcus, D., Thomas, D. Y., and Whiteway, M. (1992) The protein kinase homologue Ste20p is required to link the yeast pheromone response G-protein $\beta\gamma$ subunits to downstream signalling components, *EMBO J. 11*, 4815−4824.
28. Leberer, E., Wu, C., Leeuw, T., Fourest-Lieuvin, A., Segall, J. E., and Thomas, D. Y. (1997) Functional characterization of the Cdc42p binding domain of yeast Ste20p protein kinase, *EMBO J. 16*, 83−97.
29. Ushinsky, S. C., Harcus, D., Ash, J., Dignard, D., Marcil, A., Morchhauser, J., Thomas, D. Y., Whiteway, M., and Leberer, E. (2002) CDC42 is required for polarized growth in human pathogen *Candida albicans*, *Eukaryot. Cell 1*, 95−104.
30. Bassilana, M., Blyth, J., and Arkowitz, R. A. (2003) Cdc24, the GDP-GTP exchange factor for Cdc42, is required for invasive hyphal growth of *Candida albicans*, *Eukaryot. Cell 2*, 9−18.
31. Stevens, W. K., Vranken, W., Goudreau, N., Xiang, H., Xu, P., and Ni, F. (1999) Conformation of a Cdc42/Rac interactive binding peptide in complex with Cdc42 and analysis of the binding interface, *Biochemistry 38*, 5968−5975.
32. Gizachew, D., and Oswald, R. E. (2001) Concerted motion of a protein-peptide complex: Backbone dynamics studies of an ^{15}N-labeled peptide derived from P21-activated kinase bound to Cdc42Hs.GMPPCP, *Biochemistry 40*, 14368−14375.
33. Osborne, M. J., Su, Z., Sridaran, V., and Ni, F. (2003) Efficient expression of isotopically labeled peptides for high-resolution NMR studies: Application to the Cdc42/Rac binding domains of virulent kinases in *Candida albicans*, *J. Biomol. NMR 26*, 317−326.
34. Su, Z., Vinogradova, A., Koutychenko, A., Tolkatchev, D., and Ni, F. (2004) Rational design and selection of bivalent peptide ligands of thrombin incorporating P4−P1 tetrapeptide sequences: From good substrates to potent inhibitors, *Protein Eng., Des. Sel. 17*, 647−657.
35. Bodenhausen, G., and Ruben, D. J. (1980) *Chem. Phys. Lett. 69*, 185−189.
36. Marion, D., Driscoll, P. C., Kay, L. E., Wingfield, P. T., Bax, A., Gronenborn, A. M., and Clore, G. M. (1989) Overcoming the overlap problem in the assignment of ^{1}H NMR spectra of larger proteins by use of three-dimensional heteronuclear ^{1}H-^{15}N Hartmann−Hahn-multiple quantum coherence and nuclear Overhauser-multiple quantum coherence spectroscopy: Application to interleukin 1β, *Biochemistry 28*, 6150−6156.
37. States, D. J., Haberkorn, R. A., and Ruben, D. J. (1982) A two-dimensional nuclear Overhauser experiment with pure absorption phase in four quadrants, *J. Magn. Reson. 48*, 286−292.
38. Farrow, N. A., Zhang, O., Forman-Kay, J. D., and Kay, L. E. (1994) A heteronuclear correlation experiment for simultaneous determination of ^{15}N longitudinal decay and chemical exchange rates of systems in slow equilibrium, *J. Biomol. NMR 4*, 727−734.
39. Millet, J. O., Loria, P., Kroenke, C. D., Pons, M., and Palmer, A. G., III (2000) The Static Magnetic Field Dependence of Chemical Exchange Linebroadening Defines the NMR Chemical Shift Time Scale, *J. Am. Chem. Soc. 122*, 2867−2877.
40. Mulder, F. A., Skrynnikov, N. R., Hon, B., Dahlquist, F. W., and Kay, L. E. (2001) Measurement of slow (micros-ms) time scale dynamics in protein side chains by ^{15}N relaxation dispersion NMR

spectroscopy: Application to Asn and Gln residues in a cavity mutant of T4 lysozyme, *J. Am. Chem. Soc. 123*, 967−975.
41. Delaglio, F., Grzesiek, S., Vuister, G. W., Zhu, G., Pfeifer, J., and Bax, A. (1995) NMRPipe: A multidimensional spectral processing system based on UNIX pipes, *J. Biomol. NMR 6*, 277−293.
42. Johnson, B. A., and Blevins, R. A. (1994) *J. Biomol. NMR 4*, 603−614.
43. Dutta, K., Shi, H., Cruz-Chu, E. R., Kami, K., and Ghose, R. (2004) Dynamic influences on a high-affinity, high-specificity interaction involving the C-terminal SH3 domain of p67phox, *Biochemistry 43*, 8094−8106.
44. Nomanbhoy, T., and Cerione, R. A. (1999) Fluorescence assays of Cdc42 interactions with target/effector proteins, *Biochemistry 38*, 15878−15884.
45. Gill, S. C., and von Hippel, P. H. (1989) Calculation of protein extinction coefficients from amino acid sequence data, *Anal. Biochem. 182*, 319−326.
46. Nomanbhoy, T. K., Leonard, D. A., Manor, D., and Cerione, R. A. (1996) Investigation of the GTP-binding/GTPase cycle of Cdc42Hs using extrinsic reporter group fluorescence, *Biochemistry 35*, 4602−4608.
47. Leonard, D. A., Satoskar, R. S., Wu, W. J., Bagrodia, S., Cerione, R. A., and Manor, D. (1997) Use of a fluorescence spectroscopic readout to characterize the interactions of Cdc42Hs with its target/effector, mPAK-3, *Biochemistry 36*, 1173−1180.
48. Kramer, R. H., and Karpen, J. W. (1998) Spanning binding sites on allosteric proteins with polymer-linked ligand dimers, *Nature 395*, 710−713.
49. Kitov, P. I., Shimizu, H., Homans, S. W., and Bundle, D. R. (2003) Optimization of tether length in nonglycosidically linked bivalent ligands that target sites 2 and 1 of a Shiga-like toxin, *J. Am. Chem. Soc. 125*, 3284−3294.
50. Mulder, A., Huskens, J., and Reinhoudt, D. N. (2004) Multivalency in supramolecular chemistry and nanofabrication, *Org. Biomol. Chem. 2*, 3409−3424.
51. Jencks, W. P. (1981) on the attribution and additivity of binding energies, *Proc. Natl. Acad. Sci. U.S.A. 78*, 4046−4050.
52. Wishart, D. S., and Sykes, B. D. (1994) The ^{13}C chemical-shift index: A simple method for the identification of protein secondary structure using ^{13}C chemical-shift data, *J. Biomol. NMR 4*, 171−180.
53. Feltham, J. L., Dotsch, V., Raza, S., Manor, D., Cerione, R. A., Sutcliffe, M. J., Wagner, G., and Oswald, R. E. (1997) Definition of the switch surface in the solution structure of Cdc42Hs, *Biochemistry 36*, 8755−8766.
54. Osborne, M. J., and Wright, P. E. (2001) Anisotropic rotational diffusion in model-free analysis for a ternary DHFR complex, *J. Biomol. NMR 19*, 209−230.
55. Lee, L. K., Rance, M., Chazin, W. J., and Palmer, A. G., III (1997) Rotational diffusion anisotropy of proteins from simultaneous analysis of ^{15}N and ^{13}Cα nuclear spin relaxation, *J. Biomol. NMR 9*, 287−298.
56. Burbelo, P. D., Drechsel, D., and Hall, A. (1995) A conserved binding motif defines numerous candidate target proteins for both Cdc42 and Rac GTPases, *J. Biol. Chem. 270*, 29071−29074.
57. Guo, W., Sutcliffe, M. J., Cerione, R. A., and Oswald, R. E. (1998) Identification of the binding surface on Cdc42Hs for p21-activated kinase, *Biochemistry 37*, 14030−14037.
58. Hlavacek, W. S., Faeder, J. R., Blinov, M. L., Perelson, A. S., and Goldstein, B. (2003) The complexity of complexes in signal transduction, *Biotechnol. Bioeng. 84*, 783−794.
59. Benard, V., Bokoch, G. M., and Diebold, B. A. (1999) Potential drug targets: Small GTPases that regulate leukocyte function, *Trends Pharmacol. Sci. 20*, 365−370.
60. Rudolph, M. G., Linnemann, T., Grunewald, P., Wittinghofer, A., Vetter, I. R., and Herrmann, C. (2001) Thermodynamics of Ras/effector and Cdc42/effector interactions probed by isothermal titration calorimetry, *J. Biol. Chem. 276*, 23914−23921.
61. Song, J., and Ni, F. (1998) NMR for the design of functional mimetics of protein−protein interactions: One key is in the building of bridges, *Biochem. Cell Biol. 76*, 177−188.
62. Mammen, M., Choi, S., and Whitesides, G. (1998) Polyvalent Interactions in Biological Systems: Implications for Design and Use of Multivalent Ligands and Inhibitors, *Angew. Chem., Int. Ed. 37*, 2754−2794.
63. Kitov, P. I., and Bundle, D. R. (2003) On the nature of the multivalency effect: A thermodynamic model, *J. Am. Chem. Soc. 125*, 16271−16284.
64. Huskens, J., Mulder, A., Auletta, T., Nijhuis, C. A., Ludden, M. J., and Reinhoudt, D. N. (2004) A model for describing the thermodynamics of multivalent host−guest interactions at interfaces, *J. Am. Chem. Soc. 126*, 6784−6797.
65. Kuntz, I. D., Chen, K., Sharp, K. A., and Kollman, P. A. (1999) The maximal affinity of ligands, *Proc. Natl. Acad. Sci. U.S.A. 96*, 9997−10002.
66. Greene, L. E., and Eisenberg, E. (1980) The binding of heavy meromyosin to F-actin, *J. Biol. Chem. 255*, 549−554.
67. Davis-Harrison, R. L., Armstrong, K. M., and Baker, B. M. (2005) Two different T cell receptors use different thermodynamic strategies to recognize the same peptide/MHC ligand, *J. Mol. Biol. 346*, 533−550.
68. Li, W., Keeble, A. H., Giffard, C., James, R., Moore, G. R., and Kleanthous, C. (2004) Highly discriminating protein−protein interaction specificities in the context of a conserved binding energy hotspot, *J. Mol. Biol. 337*, 743−759.
69. Li, W., Hamill, S. J., Hemmings, A. M., Moore, G. R., James, R., and Kleanthous, C. (1998) Dual recognition and the role of specificity-determining residues in colicin E9 DNase-immunity protein interactions, *Biochemistry 37*, 11771−11779.
70. Kleanthous, C., Hemmings, A. M., Moore, G. R., and James, R. (1998) Immunity proteins and their specificity for endonuclease colicins: Telling right from wrong in protein−protein recognition, *Mol. Microbiol. 28*, 227−233.
71. Wallis, R., Leung, K. Y., Osborne, M. J., James, R., Moore, G. R., and Kleanthous, C. (1998) Specificity in protein−protein recognition: Conserved Im9 residues are the major determinants of stability in the colicin E9 DNase-Im9 complex, *Biochemistry 37*, 476−485.
72. Walker, D., Moore, G. R., James, R., and Kleanthous, C. (2003) Thermodynamic consequences of bipartite immunity protein binding to the ribosomal ribonuclease colicin E3, *Biochemistry 42*, 4161−4171.
73. Ash, J., Wu, C., Larocque, R., Jamal, M., Stevens, W., Osborne, M., Thomas, D. Y., and Whiteway, M. (2003) Genetic analysis of the interface between Cdc42p and the CRIB domain of Ste20p in *Saccharomyces cerevisiae*, *Genetics 163*, 9−20.
74. Benton, B. K., Tinkelenberg, A., Gonzalez, I., and Cross, F. R. (1997) Cla4p, a *Saccharomyces cerevisiae* Cdc42p-activated kinase involved in cytokinesis, is activated at mitosis, *Mol. Cell. Biol. 17*, 5067−5076.

BI050846L